Fundamental Photophysical Concepts and Key Structural Factors for the Design of BODIPY-based Tunable Lasers

Edurne Avellanal-Zaballa, Leire Gartzia-Rivero, Teresa Arbeloa, Jorge Bañuelos*

Dpto. Química Física, Universidad del País Vasco (UPV-EHU), Aptdo. 644, 48080, Bilbao (Spain)

Dr. Edurne Avellanal Zaballa

Dpto Química Física, UPV-EHU, Aptdo 644, 48080, Bilbao, Spain

Phone: +34 94 601 53 84

Email: edurne.avellanal@ehu.es

ORCID: 0000-0002-5218-3764

Dr. Leire Gartzia Rivero

Dpto Química Física, UPV-EHU, Aptdo 644, 48080, Bilbao, Spain

Phone: +34 94 601 59 73

Email: leire.gartzia@ehu.es

ORCID: 0000-0002-2240-4538

Dr. Teresa Arbeloa

Dpto Química Física, UPV-EHU, Aptdo 644, 48080, Bilbao, Spain

Phone: +34 94 601 59 70

Email: teresa.arbeloa@ehu.es

ORCID: 0000-0003-2737-9287

Dr. Jorge Bañuelos Prieto

*Corresponding author

Dpto Química Física, UPV-EHU, Barrio Sarriena s/n, Aptdo 644, 48080, Bilbao, Spain

Phone: +34 94 601 27 11

Email: jorge.banuelos@ehu.es

ORCID: 0000-0002-8444-4383

Abstract

This review aims to highlight the most recent and remarkable advances in our laboratory in designing efficient and long-lasting tunable dye lasers from the visible green region to the far-red-NIR edge. In recent years, we have synthesised, characterised, and applied a set of organic molecules covering this spectral region. The well-known BODIPY dye was selected as the photoactive scaffold owing to its rich and versatile chemistry. This modern dye allows deep and selective functionalization, which in turn modulates its photophysical properties. A deep understanding of the interplay between the molecular structure and photonic performance, as well as the unravelling of the key underlying photophysical mechanisms, is essential for designing photoactive dyes endowed with improved laser performance, outperforming the corresponding commercially available dyes in each spectral region. The design was focused on the chemical modification of the boron-dipyrrin core, as well as on the combination of dissimilar BODIPYs into a single molecular structure. Indeed, these complex and challenging multichromophoric assemblies exemplify a new generation of laser dyes with enhanced photonic performance. Following that, we provide an overview of the main structural and photophysical guidelines governing laser performance.

Keywords:

BODIPY, photophysical properties, dye chemistry, lasers, energy transfer, electron transfer

Introduction

We are surrounded by a broad palette of colours in nature and in our daily lives. Nowadays, natural pigments and artificial dyes are the main sources of colours [1]. Most of these are complex organic molecules, which feature a chromophore as a color-displaying unit and hence are responsible for absorbing light within the ultraviolet-visible-near-infrared (UV-Vis-NIR) spectral region. Some of them are also able to emit light and behave as fluorophores [2], which is a useful tool for gathering highly sensitive analytical information on biochemical systems [3,4] and the main photophysical process involved in many light-driven devices [5]. In addition, recent advances in organic synthesis have assisted in the design of new functional fluorophores with tailored molecular structures using well-established synthetic protocols [6,7]. Consequently, dye chemistry [8,9] has emerged as a powerful tool for the design of synthetic organic dyes with tunable photonic performance. The discovery of versatile molecular scaffolds prone to tailor-made functionalization is one of the most active and challenging currents in dye chemistry [10,11]. That is, rather than developing different dyes for each target application, choose a specific molecular structure and apply it in a variety of application fields after rational design and proper functionalization. Such tailoring of the photophysical properties of chromophores would allow the full exploitation of their potential in advanced technological applications [12,13]. Therefore, an understanding of the correlation between photophysical signatures and molecular structures is required. Knowledge of such relationships provides feedback for the design of applied fluorophores with exact and accurately predictable properties. Thus, the discovery of a single new fluorophore, while being potentially useful, is only significant in a broader sense if there is room for structural modification [14].

Undoubtedly, the paradigm of modern fluorophores is the BOron DIPYrromethene dye (trademark BODIPY, also known as “porphyrin’s little sister“).The first reports on

BODIPY date back to the 1960s, but it wasn't until the early 1990s that they gained attention thanks to the pioneering work of Boyer et al on their suitability as active media for tunable lasers [15,16]. This discovery has attracted the attention of many researchers and, as a consequence, these dyes have witnessed astonishing growth, which still holds today, as reflected by the large number of publications and patents dealing with BODIPY. This dye is classified as a cyclic cyanine, whose chromophoric core features a dipyrrin-(or dipyrromethene)-conjugated π-system chelated by a difluoroboron bridge (Figure 1). The dipyrrin framework is responsible for the main electronic transition, whereas the coordinated BF_2 unit restricts conformational flexibility, keeping it planar to enhance the aromaticity and emission efficiency because non-radiative relaxation channels related to internal conversion [17] vanish [18].

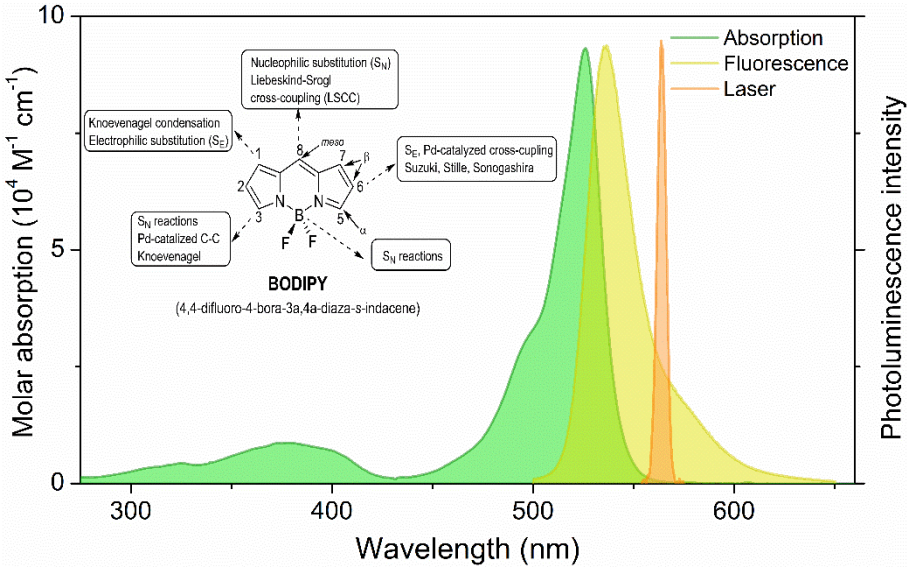

Figure 1. Scheme of the molecular structure of BODIPY core with its corresponding IUPAC numbering and main viable synthetic routes. Representative absorption, fluorescence and laser spectra in solution are also enclosed.

The desirable photophysical properties arise from this unique and chemically robust framework. They commonly display strong absorption bands, with extinction coefficients

close to 10^5 $M^{-1} \cdot cm^{-1}$, and emission bands endowed with high fluorescence quantum yields (up to 100%) and laser efficiencies (higher than 50%) in the green-yellow region of the visible electromagnetic spectrum [19] (Figure 1). These optimal characteristics are supplemented by remarkable photostability, with a reasonable tolerance to a continuous and hard irradiation regime [20-22], practically negligible population of the triplet state [23,24], and a low probability of aggregation in organic media [25,26]. However, in aqueous media, BODIPYs are not soluble, and their stability is highly reduced in extreme pH regimes (highly acidic [27] or basic). All these properties, and even the drawbacks, can be modulated or surpassed [28], respectively, owing to the chemical versatility of the boron-dipyrrin core [29,30], being readily exploitable for a multitude of synthetic routes [31-33], like Knoevenagel, Pd-mediated cross couplings, and nucleophilic substitutions, among others [34] (Figure 1). Indeed, the success of BODIPY is likely to rely on this feature, as it allows fine modulation of the photophysical properties and their exploitation in diverse photoactivatable applications.

All of these facts support and explain the extensive chemical transformations performed in BODIPY dyes over the last decades, resulting in a rich and diverse library of derivatives [35]. Indeed, these chameleonic dyes are likely the first choice when a photoactive system is required for applications demanding specific and sometimes opposite properties, being at the forefront as applied fluorophores. A quick survey of the literature reveals that BODIPYs are ubiquitous and intensively applied in lasers [36], optoelectronics [37], chiroptics [38,39], photocatalysts [40], photovoltaic devices [41,42], sensing [43-45], and diagnosis [46,47] or therapy [48-51] in biomedicine (Figure 2). The key pivotal issue is rational design to adapt the molecular structure of BODIPY to fulfil the specific photophysical properties required for each target application.

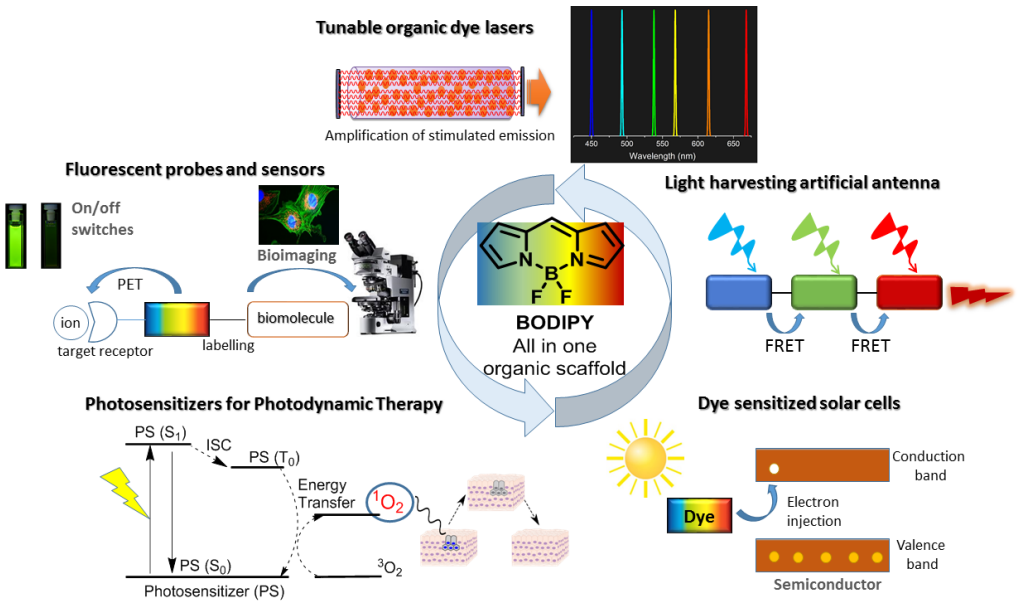

Figure 2. Scheme of representative application fields of BODIPYs.

Lasers were the first technological field in which BODIPYs were applied [52,53]. These promising results have encouraged other researchers to investigate how to improve the laser performance of photoactive media. Subsequently, two main strategies were applied. One study focused on the chemical modification of the molecular structure to enhance the photonic performance and shift the laser emission. In this approach, different functional groups were attached to the BODIPY core in an attempt to induce blue- and red-shifts to span the entire visible electromagnetic spectrum, while maintaining, or even improving, the laser efficiency and photostability in solution. Thus, electron-donor amino groups were tethered to the *meso* position yielding blue-edge laser dyes [55-57], whereas π–extended BODIPYs decorated with aromatic moieties and aza-BODIPYs with the central carbon replaced by nitrogen were tested to promote the opposite shift and develop red-edge lasers [58,59]. Another approach was based on embedding the dye in suitable solid hosts to develop solid-state dye lasers (SSDL) [54]. In this approach, the solvent is replaced with solid matrices. Thus, SSDL are environmentally friendly, compact [54,60], and improve the photostability of

guest dyes owing to the cage-protecting effect of the surrounding solid and rigid host. To this end, BODIPY dyes have been incorporated as dopants in polymers (linear, branched, crosslinked), inorganic hosts (sol-gel materials), and nematic liquid crystals [61].

In this regard, the development of novel BODIPY dyes for laser applications has been one of the main research areas in recent years. During this period, we focused on understanding the complex interplay between molecular structure and photophysical properties. Such knowledge has enabled deep but controlled modulation of their photonic performance and the development of improved dye lasers, ousting those based on commercially available dyes across the entire visible spectral window. Herein, we provide an overview of the main photophysical guidelines that trigger the photonic performance of dye lasers based exclusively on BODIPY. Special emphasis is placed on spanning the emission toward long wavelengths, an appealing region for telecommunications and biomedicine. In particular, we applied three main structural approaches (Figure 3) to modulate laser performance (*i*), spectral shift (*ii*), and photostability (*iii*):

i. Chemical modification of the boron bridge: Replacement of fluorine atoms at the boron centre with moieties with different stereoelectronic features.

ii. Extension of π–conjugated dipyrrin: The fusion or linkage of aromatic frameworks at the BODIPY or aza-BODIPY core enables a pronounced bathochromic spectral shift for the development of red-edge and NIR lasers.

iii. All-BODIPY-based multichromophores: The most suitable red-emitting BODIPYs were used as energy acceptor scaffolds to anchor energy donors BODIPY at the dipyrrin core or boron centre of the former to design long-wavelength emitting energy transfer dye lasers (ETDL).

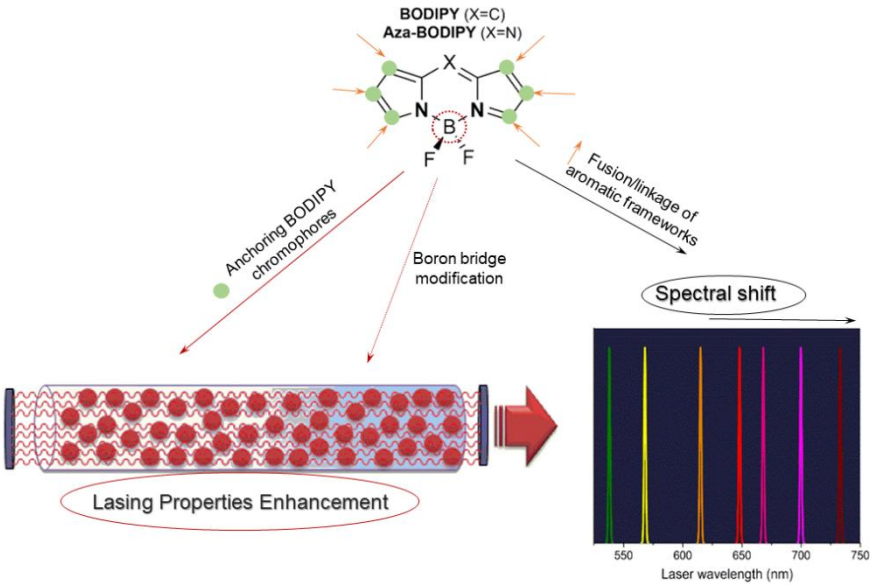

Figure 3. Schematic view of the conducted chemical modifications onto the BODIPY and aza-BODIPY cores to develop wavelength-tunable dye lasers towards the red-edge and NIR spectral regions.

1. Modifications at the Boron Centre: Enhancement of Laser Properties

BODIPY functionalization has been explored using several synthetic routes [34]. These transformations usually involve the chemical modification of the carbon skeleton. The direct functionalization of BODIPYs at the boron centre has not been evaluated in depth hitherto [62-64], and a limited number of new derivatives have been obtained thus far [65]. Nevertheless, such at-boron chemistry deserves recognition as a strategy for chromophoric position [66-69] to enhance water solubility [70], improve biorecognition of targets [71], and ameliorate laser photostability [72].

Although the boron atom does not participate in the delocalised π-system, the replacement of the highly electronegative fluorine atoms (*F*-BODIPYs) by moieties with different electron-withdrawing behaviours could rearrange the electronic density at the chromophore. Moreover, such atom exchange usually causes a noteworthy drop in the stability of the dyes because the electron density at the boron atom increases, thus reducing its

Lewis acidity and reducing its capability to be chelated by the dipyrrin moiety. To improve this handicap, electron-poor functional groups have been mainly employed [73] via nucleophilic substitutions with certain alkyl and alcoxy-based moieties, leading to the corresponding *C*- and *O*-BODIPYs, respectively [73-76]. However, nitrogen is also an appealing candidate for replacing the at-boron fluorine atoms because its structural and electronic properties are between those of carbon and oxygen. Synthetic access to *N*-BODIPYs is challenging because of the electron-rich nature of the amino groups. However, stabilisation of the involved diaminoboron chelate is viable by adding tosyl substituents at the nitrogen atoms to reduce the electron-donating ability of the amines [77]. Unlike *C*- and *O*-BODIPYs, *N*-BODIPYs enable broad post-functionalization (up to three substituents or even quarterisation) owing to key nitrogen atom bonding features such as higher reactivity, different bond directionality, and enhanced bond valence.

In the following lines, we disclose the photophysical and lasing properties of a set of *C*-BODIPYs (**1** and **4**) [78], *O*-BODIPYs (**5** and **7**) [69] and *N*-BODIPYs (**8** and **10**) [77] sharing the same chromophoric core (commercial *F*-BODIPY known as PM567) but differing in the stereolectronic properties of the at-boron pendant moieties (Figure 4). We aimed to gain deeper insight into the role of the electronic properties and steric factors of such functionalization on the photophysical properties and determine the most suitable modification for laser purposes.

The position and profile of the spectral bands of the at-boron-modified BODIPYs are roughly those of their *F*-BODIPY counterparts. Nonetheless, the electronic properties of the group anchored to the boron atom played a key role in the fluorescence response. The replacement of fluorine atoms by weak electron acceptor groups, such as acetylene in **1** (Hammet parameter [79] σ_p = 0.18) or acetoxy in **5** (σ_p = 0.31), provides a fluorescence efficiency similar to that of the parent PM567 (Figure 4). However, a further increase in the

electron-withdrawing properties of the anchoring cyano in **2** (σ_p = 0.66) or trifluoroacetoxy in **6** (σ_p = 0.46) improved the fluorescence response (Figure 4).

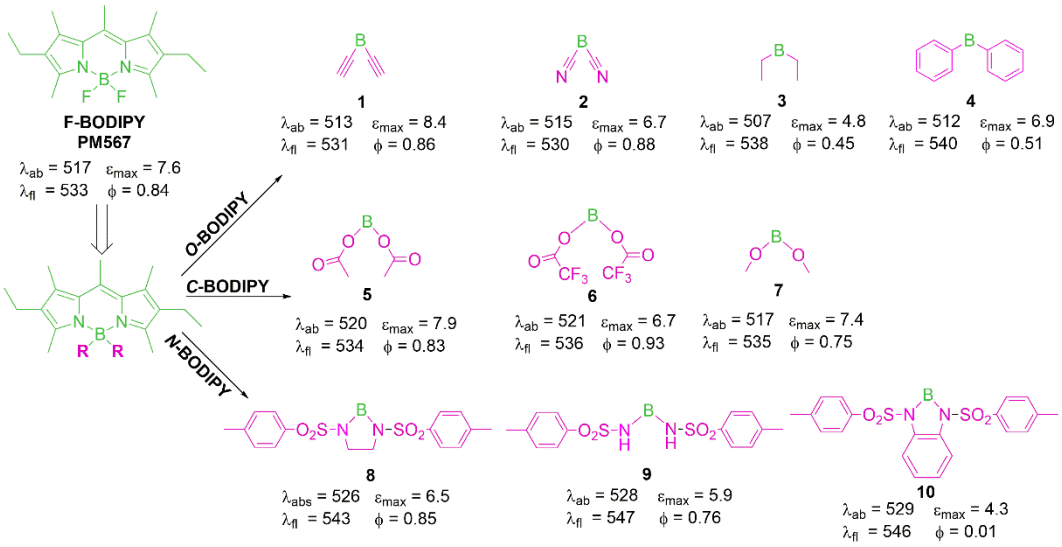

Figure 4. Representative *C*-, *O*- and *N*-BODIPYs derived from commercial *F*-BODIPY PM567 and their corresponding main photopysical properties in ethyl acetate. Absorption (λ_{ab}) and fluorescence (λ_{fl}) wavelengths (in nm), molar absorption (ε_{max}, in $10^4 \cdot M^{-1}$ cm^{-1}) and fluorescence quantum yield (ϕ).

The electronic rearrangement caused by this type of substitution results in increased aromaticity in the chromophore, as evidenced by the lower Bond Length Alternation (BLA) parameter in the chromophoric π-system (Figure 5) [80]. *C*- and *O*-BODIPYs **2** and **6**, respectively, are more aromatic and display lower BLA values (0.023 and 0.019) than their corresponding counterparts bearing weak electron-withdrawing groups (compounds **1** (0.027) and **5** (0.024), respectively). Further evidence of this relationship is gained by the recorded reduction in the fluorescence efficiency when electron donor groups, such as ethyl in **3** (σ_p = -0.15) or metoxy in **7** (σ_p = -0.27), replace the fluorine atoms (ϕ = 0.45 and 0.73 in ethyl acetate, respectively), in good agreement with the observed enhancement in the BLA parameters (0.031 and 0.026) (Figure 5) [69,78]. Another remarkable issue is conformational freedom. Thus, unconstrained rings (such as phenyl in **4**) with free motion appended at the

boron atom enhance the non-radiative deactivation channels related to internal conversion, as reflected in the deleterious effect on fluorescence (down to 0.51 also in ethyl acetate, Figure 4). The influence of both electronic and steric factors is also reflected in *N*-BODIPYs bearing a tosilated diamino. Thus, compound **8** bearing a boron-shared five-membered constrained spiranic ring, showed higher fluorescence quantum yields than its non-spiranic counterpart, **9** with higher conformational freedom. Furthermore, the fusion of a phenyl group at the spiranic ring in **10** leads to an electron-rich moiety that can switch on photoinduced electron transfer (PET) from the pendant diaminoboron moiety to the dipyrrin core, inducing a drastic loss of the fluorescence signal (Figure 4) [77].

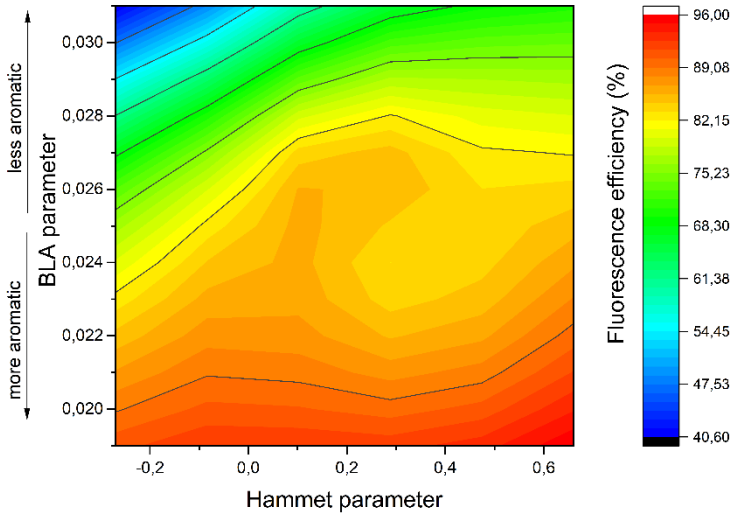

Figure 5. Evolution of the fluorescence efficiency with the BLA and Hammet parameter, which account for the aromaticity of the chromophore and electron donor/acceptor properties of the substituent, respectively.

These improvements in the photophysical properties upon tailor modification of the boron centre have a marked impact on the lasing properties. The lasing efficiencies of these chromophores were studied by pumping at 532 nm wavelength. All the at-boron-modified BODIPYs with optimal electron-withdrawing properties and restricted conformation showed higher laser efficiency than the commercial parent dye PM567 (Figure 6), reaching values of

around 70% (fluorine replaced by cyano, dye **2,** and trifluoroacetoxy, dye **6**). Both dyes have the brightest fluorescence response, although it should be mentioned that the increase in laser efficiency is more marked than that predicted from the photophysical properties. All of them are far more photostable than the commercial dye PM567, being able to withstand long lasting periods of strong and prolonged irradiation (Figure 6). Again, the dyes showing the best laser efficiency were the most photostable **2** and **6**, whose laser-induced fluorescence emission remained at the initial level after 100000 pulses. Indeed, such a marked increase in photostability upon replacement of the at-boron fluorine atoms could explain the noticeable improvement in the laser efficiency, which was not reflected in the fluorescence efficiency. The lower photobleaching in the gain media upon laser pumping implies a reduction in the losses in the resonator cavity and facilitates the attainment of the laser threshold.

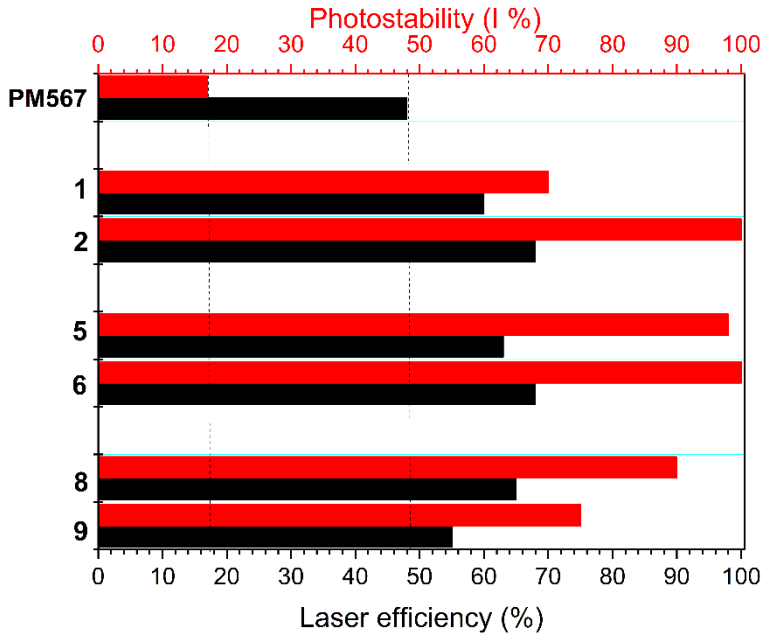

Figure 6. Lasing efficiency and photostability (intensity of the laser output after 100000 pump pulses with respect to its initial intensity, I (%) = (I/I_0) x 100) of representative *C*-, *O*-, and *N*-BODIPYs with respect to its *F*-BODIPY precursor in ethyl acetate at the optimum dye concentration (from 1.50 to 3.50 mM).

2. Modifications at the Dipyrrin Core: Far-Red and NIR Dyes

Among the frequencies of radiation furnished by the electromagnetic spectrum, photons corresponding to the red-edge of the visible and NIR regions are indispensable in technological fields such as telecommunications and biomedicine, owing to the ability of this radiation source to travel over long distances and its low interference with the surroundings [81-84]. The regions 650-900 nm (the so-called "biological window") and 800-1600 nm (the "telecom range") are particularly appealing for both applications. In biomedicine, this type of light penetrates more deeply into biological tissues (up to 2-5 cm) and minimises photo-damage of the samples. In addition, it enhances the resolution of bioimaging because background interference related to the autofluorescence of surrounding biomolecules is avoided [85]. In technology, fibre optics enables communication and optical spectroscopy on sites that are conventionally inaccessible owing to the large distances required [86]. Therefore, the design of photoactivatable molecules displaying efficient and long-lasting fluorescence signals in the red-NIR spectral window is of paramount importance in biotechnology.

Organic dyes are suitable for this purpose because of their chemical versatility [87]. However, for the laser purposes addressed herein, a number of parameters and signatures must be considered in molecular design. The prototype dye should display bright emission efficiencies at long wavelengths together with high photostability under intense irradiation conditions. At present, most commercially available dyes in this spectral region are based on the cyanine skeleton [88]. These dyes emit deep in the red-NIR region, but they have some drawbacks related to: (*i*) tedious synthetic and purification procedures; (*ii*) low fluorescence efficiency (owing to conformationally flexible structures which promote non-radiative deactivation funnels further favoured by their intrinsic push-pull character [89]); (*iii*) poor

photostability due to photobleaching; and (*iv*) limited chemical versatility for post-functionalization.

In this scenario, the search for new molecular structures with the reddest spectral bands while maintaining or improving the efficiency of the emission signal and its tolerance under prolonged exposure to intense irradiation is still challenging [90]. To this end, we propose three different approximations to render red and NIR lasers, based on modifications of the BODIPY core (Figure 7). To achieve a large bathochromic shift, the HOMO-LUMO gap should be reduced by extending the conjugation through the aromatic frameworks [19]. These aromatic rings can be either fused to the dipyrrin core (benzofuran), leading to conformationally restricted BODIPYs, or connected to the core via a single bond, enabling resonant interactions between the dipyrrin and these peripheral groups (phenyls, styryls, and anisoles) [91,92]. Moreover, inspired by the structural changes undertaken in porphyrines to obtain phthalocyanines, the *meso* carbon can be replaced by a nitrogen atom, leading to aza-BODIPYs [93]. This simple modification induces a pronounced redshift [94]. Indeed, the aza-BODIPY dye family stands out as a promising alternative for designing bright, stable, compact, and small NIR emitters [95].

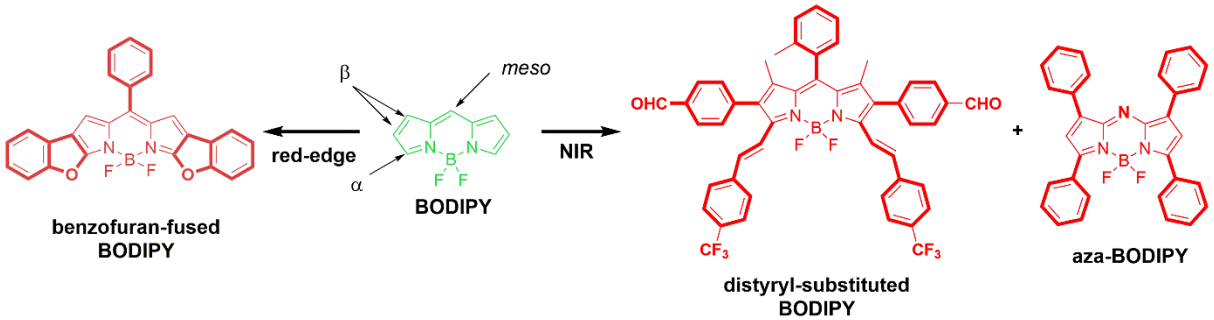

Figure 7. BODIPY-based approaches to push spectral bands towards the red-edge of the visible spectrum and the NIR region.

2.1. Benzofuran-Fused BODIPYs

The fusion of benzofuran rings to the positions 2, 3 and 5, 6 of the dipyrrin core spans the aromaticity. Consequently, strong bathochromic shifts of the spectral bands (placed at 580 nm and approaching 600 nm in absorption and fluorescence, respectively, for dye **11**) and higher absorption probability (molar extinction coefficients up to $17 \cdot 10^4$ $M^{-1} \cdot cm^{-1}$) were induced with regard to the pristine BODIPY or derivatives described in Section 1 (Figure 8 and 9). In fact, theoretical calculations predict a π-system delocalised through all the conjugated aromatic rings, except the *meso*-aryl ring, owing to its twisted disposition (around 80º respect to the BODIPY-core plane, Figure 9 inset). In addition, this set of dyes (e.g. **11** and **12**) are extremely fluorescent ((ϕ > 90%, Figure 8), independent of the substitution pattern and solvent polarity [96]. These dyes are characterised by a high conformational restriction and planar geometry due to the cyclisation of the substituent, which hinders geometry relaxation upon excitation (small Stokes shifts, $\Delta\nu_{St} \approx 350$ cm^{-1}), lowering the non-radiative deactivation pathways. Furthermore, the extension of the π-system through the aromatic fused rings displaces the electronic density far from the key *meso* position, preventing the quenching pathway related to the free motion of the unconstrained 8-phenyl [97]. The fusion of more rings to benzofuran (**13**, which comprises up to seven aromatic rings), implies an additional bathochromic shift, reaching fluorescence bands centred at 625 nm but less intense (ϕ down to 70% (Figure 8). It is likely that the geometrical stress to maintain such large aromatic rings in the plane induces slight bending, which favours internal conversion relaxation.

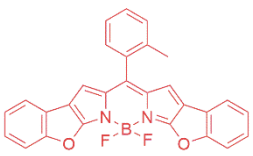

11

λ_{ab} = 582 ε_{max} = 16.9
λ_{fl} = 595 ϕ = 0.93
λ_{la} = 649 %Eff = 48

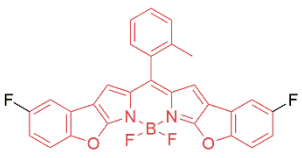

12

λ_{ab} = 576 ε_{max} = 12.7
λ_{fl} = 587 ϕ = 0.93
λ_{la} = 642 %Eff = 43

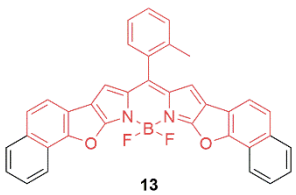

13

λ_{ab} = 607 ε_{max} = 10.0
λ_{fl} = 626 ϕ = 0.69
λ_{la} = 685 %Eff = 27

Figure 8. Representative benzofuran-fused BODIPYs with their corresponding main photophysical and laser properties in ethyl acetate. Absorption (λ_{ab}) and fluorescence (λ_{fl}) wavelengths (in nm), molar absorption (ε_{max}, in $10^4 \cdot M^{-1}$ cm^{-1}), fluorescence quantum yield (ϕ), laser wavelength (λ_{la}, in nm) and efficiency (%Eff).

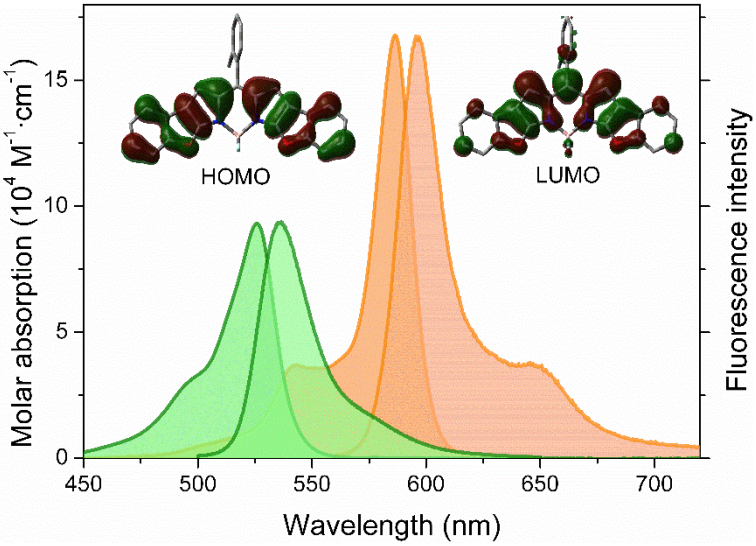

Figure 9. Absorption and normalized fluorescence spectra of a representative benzofuran-fused BODIPY (**11**, in orange) compared with the pristine BODIPY (green) in a common solvent. The corresponding molecular orbitals of the former are enclosed to highlight the π-extension.

In agreement with their high fluorescence efficiency, these dyes display a strong laser emission, the position of which markedly depends on the dye concentration and pump energy (Figure 8 and 10). Thus, at low concentrations or low pump energies, the laser signals appear in the expected position (615 nm, reaching 640 nm for the more π–extended dye **13**), where the spectral overlap between the absorption and fluorescence profiles is almost negligible. However, at high concentrations, the laser signal was more red-shifted, reaching 650 nm for dye **11** and 685 nm for dye **13** (Figure 10). These laser emission lines appear further away from the absorption and fluorescence signals (approximately 70 nm and 50 nm bathochromically shifted, respectively) than typically expected for BODIPY dyes

(approximately 40 nm and 20 nm, respectively) [69]. Thus, this trend cannot be attributed to enhanced reabsorption and reemission phenomena. Moreover, dual laser emission can be achieved by adjusting the dye concentration (between 0.25 - 0.50 mM). Fluorophores with flat molecular geometries are prone to stacking, leading to the formation of aggregates. Under soft conditions (such as those used for the recording of photophysical properties), no sign of aggregation was detected even at millimolar concentrations. Thus, the high pump energy in high-optical-density active media enables the formation of excited-state aggregates (photoinduced excimers or superexciplexes) [98]. Therefore, the laser emission recorded at long wavelengths corresponds to an aggregated state because it is detected at higher optical densities, whereas that recorded at shorter wavelengths corresponds to the expected monomeric form (Figure 10). As a result, it is possible to widen the tuning range window [99] using the dye concentration or pump energy.

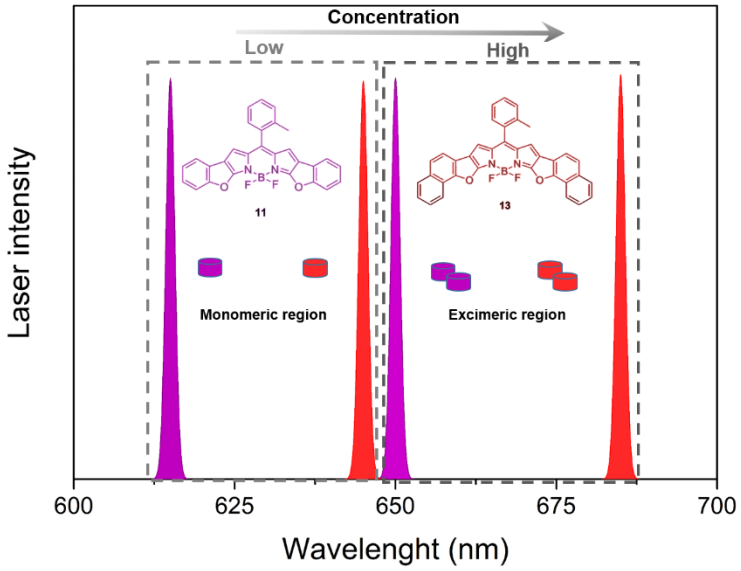

Figure 10. Laser spectra (dual emission depending on the dye concentration) of dye **11** (purple) and **13** (red) in ethyl acetate.

According to the fluorescence parameters, high lasing efficiencies (approaching 50% at high concentrations) were recorded for those dyes showing higher fluorescence

efficiencies, which were lower for the more extended dye **13** (down to 27%, Figure 8). The amount of energy required to reduce the laser induced fluorescence by 10% (that is, to retain 90% of the initial signal) is 3.3 and 4.5 GJ·mol^{-1} for **11** and **13** respectively), increasing up to 7.4 GJ·mol^{-1} for the fluorinated dye **12**. Thus, the stability afforded by the strongly bound fluorine atoms is a successful strategy to further boost the photostability and, hence, the operative lifetime [100]. To contextualise these results, we compared them with the commercially available BODIPY dye in the red region, PM650 [101], which bears a cyano group at the *meso*-position of the permethylated core. Because it reduces the reactivity against ambient oxygen, which is involved in the photo-oxidative degradation mechanism [102], this electron withdrawing functionalization yields a high photostability (6.3 GJ·mol^{-1}), but it reduces the lasing efficiency (down to 30%) due to the promotion of charge transfer phenomena. Therefore, fluorinated benzofuran-fused BODIPY **12** improves the lasing performance at the red edge, both in terms of efficiency (43%) and photostability.

2.2. Styryl-BODIPYs

A very effective approach to deepen the spectral bands toward the red edge of the visible region is the extension of the chromophoric π-conjugated system through aromatic moieties linked to the core, especially at the α-positions 3 and 5. Accordingly, we designed π-extended BODIPYs bearing triazoles or phenyls at positions 2 and 6, and in particular, styryls at the key positions, as the main functionalization drove the pursuit bathochromic spectral shift (Figure 11).

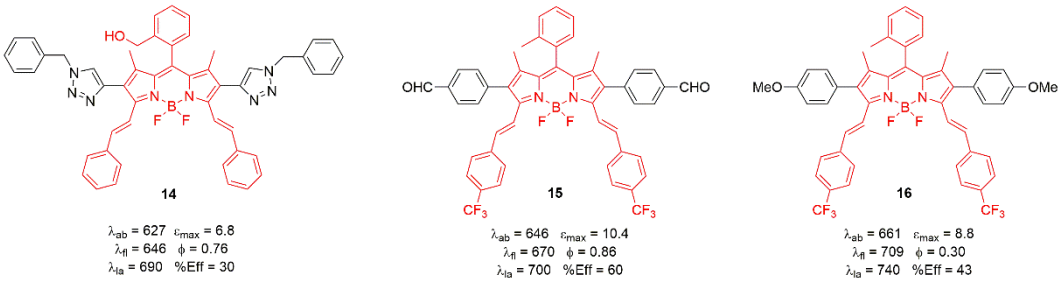

Figure 11. Distyryl-substituted BODIPYs and their corresponding main photophysical and laser properties in ethyl acetate. Absorption (λ_{ab}) and fluorescence (λ_{fl}) wavelengths (in nm), molar absorption (ε_{max}, in $10^4 \cdot M^{-1}\ cm^{-1}$), fluorescence quantum yield (ϕ), laser wavelength (λ_{la}, in nm) and efficiency (%Eff).

The bathochromic shift induced by styryls is more pronounced than that upon fusion of aromatic rings (section 2.1), and it can be enlarged if the 2,6-triazol groups of **14** are replaced by phenyls in **15**. Indeed, this dye displays an absorption band centred at around 645 nm with a high molar absorption coefficient (exceeding 10^{-5} $M^{-1} \cdot cm^{-1}$, Figure 11) as a result of a more effective extended conjugation, supported by theoretical calculations (Figure 12). Indeed, the transition from the HOMO to the LUMO entails electronic charge transfer from the pendant aromatic units to the dipyrromethene core, mainly from those at the positions 2 and 6, whose contribution to the LUMO is almost negligible [103]. It is noteworthy that the additional strong UV absorption was located at 350 nm (Figure 12), a trademark of 3,5-styryl substituted BODIPYs, and theoretically attributed to the interaction between the styryl groups and chromophoric pyrroles [97]. Accordingly, distyryl-substituted BODIPYs show a strong emission (beyond 650 nm) endowed with a high fluorescence efficiency (approaching 90%, Figure 11). A priori poorer fluorescence ability can be expected, as the emission is progressively red-shifted according to the energy gap law. Indeed, a low energy gap increases the overlap between the vibrational levels of the ground and excited states and therefore favours non-radiative relaxation related to internal conversion. However, such a lowering

might also increase the radiative rate constant (up to $1.9 \cdot 10^8$ s^{-1} in these dyes), counteracting the moderate increase in the non-radiative constant (lower than $0.6 \cdot 10^8$ s^{-1}). Consequently, the fluorescence lifetimes (approximately 4.5 ns) resemble those recorded for typical BODIPYs operating in spectral regions with higher energy gaps.

To further increase the spectral shift, a push-pull effect was induced by the insertion of electron donor (methoxy) and acceptor (trifluoromethyl) groups at the aromatic moieties placed at 2,6 and 3,5 positions, respectively (**16**, Figure 11). Indeed, both functionalizations induced a prominent red-shift in the emission (located at 710 nm). However, the fluorescence response becomes sensitive to solvent polarity (the efficiency decreases from 61% to 13% in polar media) [97]. The simultaneous presence of electron donor and withdrawing entities in the same structure strengthens the formation of intramolecular charge transfer (ICT) process [92]. The energy of the ICT states depends significantly on the solvent polarity. Thus, in polar media, the photoinduced charge separation is further stabilised, and the ICT becomes the low-lying state, quenching the emission from the locally excited (LE) state. Therefore, push-pull dyes are a suitable alternative for achieving long-wavelength emission; however, in exchange, the fluorescence response decreases.

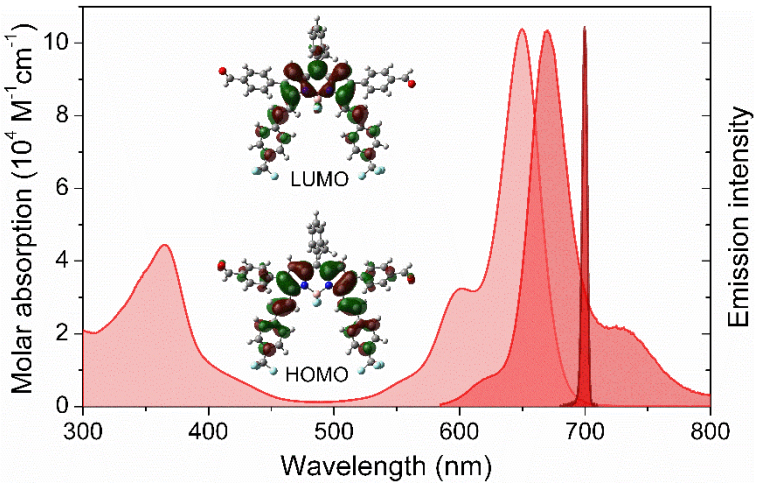

Figure 12. Absorption, fluorescence and laser spectra of representative styrylated BODIPY **15** in solution. The corresponding HOMO and LUMO orbitals are also enclosed to highlight the π-extension.

The lasing properties correlated well with the photophysical signatures, and dye **15** provided NIR emission (700.0 nm) and the most efficient signal (up to 60%, Figure 11). In addition, it was highly photostable, maintaining its initial laser output without any sign of degradation after 50000 pulses at a repetition rate of 10 Hz. To put this result into perspective, we measured the commercially available oxazine Nile Blue (NB), which is located in the same region and under the same conditions. NB not only shows a lower lasing efficiency (around 33%) than the previously reported dyes, but is also far more unstable than the styryl-substituted BODIPYs because it is completely bleached just after 8000 pulses. Moreover, the high absorption at the pump wavelengths of dyes **14** and **15** reduces the required gain-media concentration in comparison with NB (from 10 mM to 2 mM), preventing dye solubility problems and aggregation. Therefore, styrylated BODIPYs are highly recommended photoactive media for efficient and long-lasting laser emission at the far-red-NIR edge.

2.3. Polyarylated Aza-BODIPYs

Replacement of the central *meso*-carbon of BODIPY by an aza group is an appealing way to induce red shifts without increasing the molecular size [94]. This minimal structural change lowers the energy gap owing to the LUMO stabilisation induced by the electronegative *meso*-nitrogen [93,94]. In previous sections, we stated that the linkage of aromatic moieties was more successful in inducing pronounced bathochromic shifts than their fusion. Thus, peripheral aromatic substituents were grafted onto the aza-BODIPY scaffold (Figure 13) to achieve absorption and emission in the NIR region.

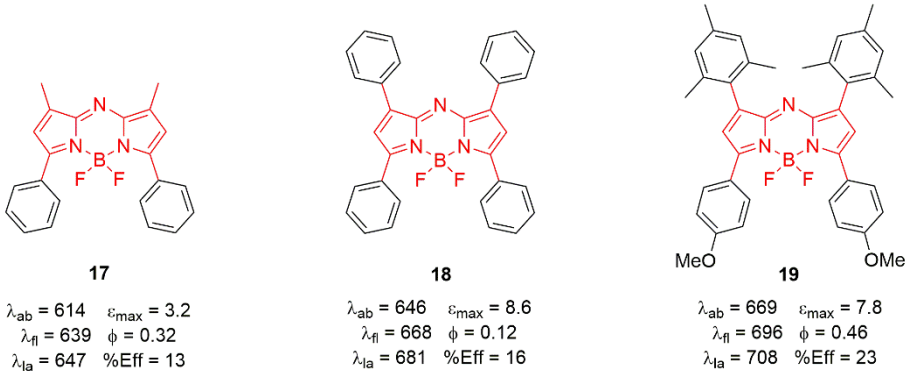

Figure 13. π-extended aza-BODIPYs and their corresponding main photopysical and laser properties in ethyl acetate. Absorption (λ_{ab}) and fluorescence (λ_{fl}) wavelengths (in nm), molar absorption (ε_{max}, in $10^4 \cdot M^{-1}\ cm^{-1}$), fluorescence quantum yield (ϕ), laser wavelength (λ_{la}, in nm) and efficiency (%Eff).

In agreement with the conclusions reached in Section 2.2., the aza-BODIPY-bearing phenyls decorated with electron donor groups (anisoles) display the reddest absorption and fluorescence (reaching almost 670 and 700 nm, respectively, for dye **19** in Figure 14). Although the aromatic rings at positions 1 and 7 have minor impacts (or negligible if mesityls are added) in the conjugated π–system, 3,5 functionalization of aza-BODIPY with anisoles is sufficient to induce a pronounced reduction in the energy gap and the ensuing bathochromic shift without further functionalization at positions 2 and 6 (Figure 13). Again, the conformationally restricted dye **19** (see the constrained mesityl) displays higher fluorescence efficiency than its counterparts **17** and **18** (see the free motion of the phenyl), reaching 46% (Figure 13), albeit its drops in polar/protic solvents (down to 20%). The replacement of the *meso*-carbon by electronegative nitrogen results in a pronounced rearrangement of the electronic distribution along the chromophore core. Indeed, such *meso*-aza becomes negatively charged (partial charge ranging from -0.45 to -0.64) and is readily available to create hydrogen bonds with alcohols, which could increase the non-radiative deactivation channels related to internal conversion (geometry bending and planarity losses). Compared

with the red-BODIPYs detailed in sections 2.1 and 2.2, aza-BODIPYs are less fluorescent. However, the aza modification provides a more effective red-shift (Figure 13), and hence the loss of fluorescence (expected in terms of the energy gap law as the spectral bands are located at longer-wavelengths) is assumable.

To ameliorate the fluorescence response of aza-BODIPY, we applied the same strategy described in section 1, that is, replacing the fluorine atoms of *F*-aza-BODIPYs by functionalizations that yielded the best photonic performance in *F*-BODIPYs, cyano, and trifluoroacetoxy (*C*- and *O*-aza-BODIPYs). Surprisingly, such an at-boron chemical modification did not result in any remarkable improvement in the fluorescent response. Moreover, most *C*- or *O*-aza-BODIPYs were photobleached with ageing time. It is likely that this low chemical stability is related to the lower stability of the chelate of aza-dipyrrin by boron [104]. This finding supports the aforementioned different electronic distributions of the aza-BODIPY and BODIPY cores and suggests that the more suitable functionalization of boron should be adjusted depending on the substitution pattern of the dipyrrin core.

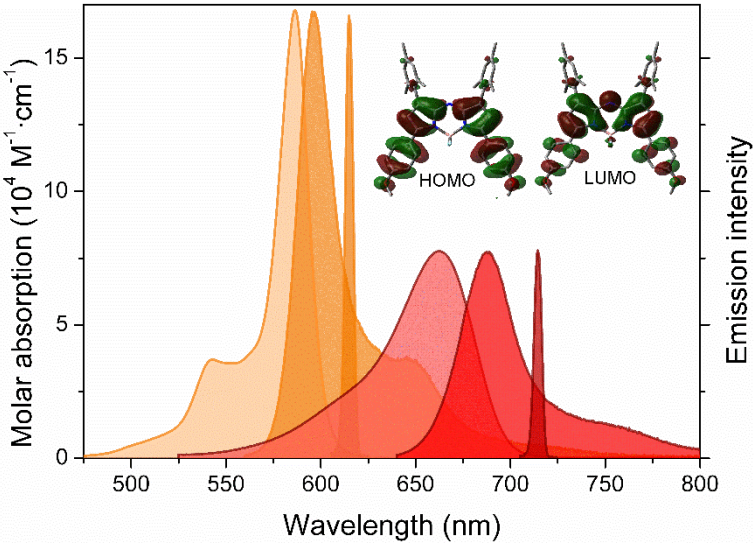

Figure 14. Absorption, fluorescence and laser spectra of representative polyarylated aza-BODIPY **19** (red) compared with the benzofuran-fused BODIPY **11** (orange) in a common media. The corresponding HOMO and LUMO orbitals of **13** are also enclosed.

These aza-BODIPYs show laser emission deep in the red edge of the visible spectrum, from 650 nm to 710 nm (Figure 14), reaching the NIR with laser efficiencies ranging from 10% to 23% in dye **19**, which correlates well with the fluorescence signatures. Strikingly, the most photostable aza-BODIPYs were those with lower lasing efficiencies. All of them required at least an energy dose of 10 $GJ \cdot mol^{-1}$ to reduce the laser-induced fluorescence by 10%. In particular, dye **18** withstood up to 47 $GJ \cdot mol^{-1}$, exhibiting the same drop. This dye, in particular, exhibits modest emission efficiency (both in fluorescence and laser) due to the conformational freedom provided primarily by the free motion of the 1,7-phenyl, but such motion can dissipate excess energy during the pumping process in the resonator cavity, resulting in greater endurance under hard irradiation regime. To put these results in context, we again compared aza-BODIPYs with commercial NB. Although the laser efficiencies of aza-BODIPYs are lower, their photostability is much better (limited to just 10 $GJ \cdot mol^{-1}$ in NB), being four times higher in case of dyes **17** and **18** (44 and 47 $GJ \cdot mol^{-1}$, respectively).

Therefore, BODIPYs are suitable scaffolds for designing a chart of photoactive dyes applied as efficient and stable tunable lasers within the spectral window of 615–710 nm. In particular, benzofuran-fused BODIPYs are suitable for the red edge, whereas styrylated BODIPYs and poliarylated aza-BODIPYs reach the far-red-NIR spectral region (Figure 15).

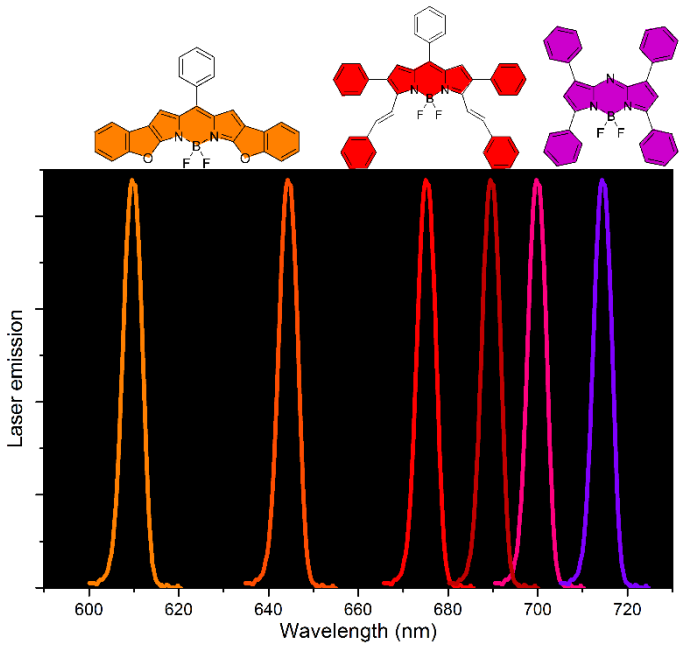

Figure 15. Laser emission tuning range available by the BODIPY-based laser dyes in the red-NIR spectral window.

3. Multichromophores as Energy Transfer Lasers

Thus far, we have focused on highly functionalized simple BODIPY dyes with improved photonic signatures. Conformationally restricted molecular structures with low geometrical rearrangements upon excitation were tested to ensure high emission efficiencies and avoid undesirable nonradiative relaxation channels. Thus, these dyes feature a small Stokes shift, which enhances the reabsorption/re-emission phenomena. In addition, the absorption is restricted to a narrow spectral region and the photostability is limited owing to the intrinsic organic nature of the dye. To offset such shortcomings, the exploration of multichromophores has emerged as an appealing alternative for designing the next generation of laser dyes [105-107]. To this end, dyes with absorption/emission in complementary regions and able to undergo excitation energy transfer (EET) are covalently linked through suitable spacers to allow broadband and simultaneous absorption of incoming light.

A rational molecular design is mandatory to build these energy transfer cassettes, and some key parameters must be considered, such as (*i*) spectral overlap between the donor and acceptor emission and absorption bands, (*ii*) short interchromophoric distances, (*iii*) fine control over their relative orientation, and (*iv*) steric effects to retain the molecular identity of the molecular units after the linkage. If the design is adequate, highly efficient intramolecular EET processes can occur, owing to the imposed short donor-acceptor distances by the covalent linkage between the donors (energy migration or homo-EET) and finally reaching the emitting acceptor trap (hetero-EET).

Actually, photonic antennae mimicking photosynthesis are widely used in imaging [108,109] and photosensing of solar cells [110], luminescent solar concentrators [111], light modulators in white-light emitting systems [112], and tunable dye lasers [113], with the latter being the focus of this review. In this regard, energy-transfer cassettes enable a more versatile selection of the pumping source, and photodegradation is further reduced because the final emitting chromophoric unit can be indirectly excited through EET from the donor [114,115].

Hence, in this section, we provide an overview of the recent advances carried out in our laboratory using multichromophoric photoactive media to render red-emitting energy transfer lasers. To this end, we selected the long-wavelength emitting dyes described in sections 2.2 and 2.3 as energy acceptors in which a suitable energy donor based on BODIPY has been appended. In particular, aza-BODIPYs (Section 3.1) and styrylated BODIPYs (Section 3.2) bear peripheral BODIPYs, leading to all-BODIPY-based triads, pentads, and hexads. We analysed the impact of the spacer, linkage position, and number and type of donor and acceptor moieties on the final energy transfer efficiency of the cassettes, as well as the role of competing electron transfer processes and their modulation with the stereoelectronic properties of the building blocks.

3.1. Aza-BODIPY-BODIPY Cassettes

The performance of aza-BODIPY dyes as NIR emitters is discussed in section 2.3. Accordingly, we chose **18** as the energy acceptor moiety to attach green-emitting BODIPYs as energy donors at the boron bridge and dipyrrin core (Figure 16).

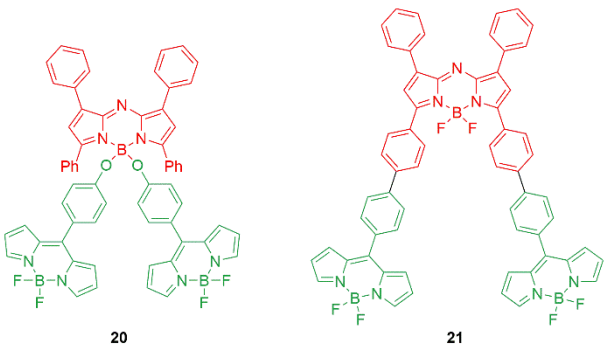

Figure 16. Structure of aza-BODIPY-BODIPY based cassettes together with their corresponding main photophysical and laser properties in ethyl acetate. Absorption (λ_{ab}) and fluorescence (λ_{fl}) wavelengths (in nm), molar absorption (ε_{max}, in $10^4 \cdot M^{-1}$ cm^{-1}), fluorescence quantum yield (ϕ), laser wavelength (λ_{la}, in nm) and efficiency (%Eff).

The absorption profile features two clearly discernible absorption bands located in the visible region (Figure 17): the prevailing one localised at higher energies and ascribed to the two pendant BODIPY chromophores (around 500 nm) and the other at lower energies belonging to the π-extended aza-BODIPY (around 650-680 nm if the central dye is decorated with 3,5-phenyl or biphenyl, **20** and **21**, respectively). Hence, the linkage of the donor through its *meso* position is suitable to ensure that each chromophoric subunit retains its molecular identity after the linkage because the 8-phenyl is twisted, avoiding electronic couplings with the dipyrrin core. Indeed, computational simulations also predicted two main transitions whose molecular orbitals are located in each chromophoric fragment (Figure 17).

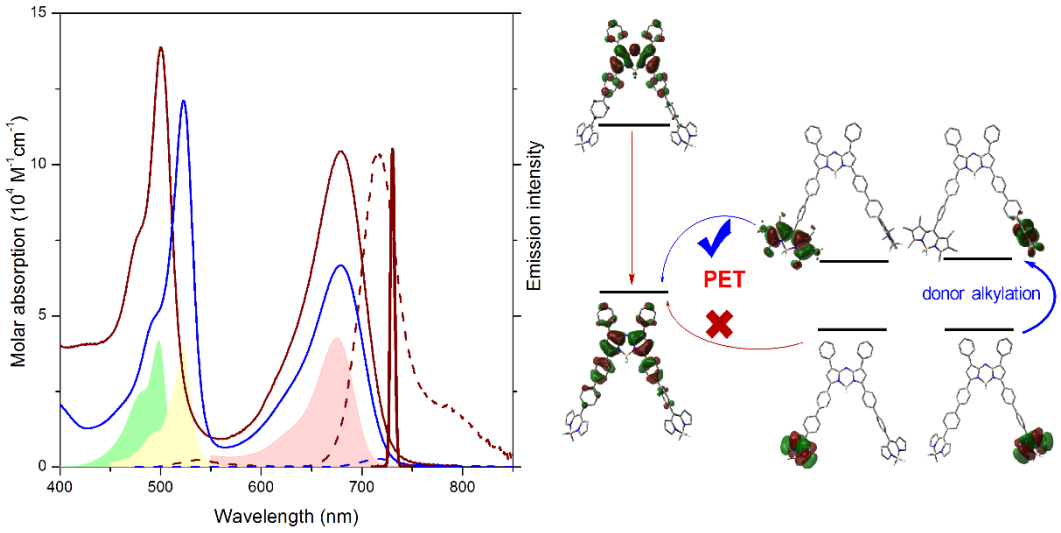

Figure 17. Absorption (solid lines), fluorescence (dashed lines, after selective excitation at the BODIPY donor) and laser spectra of cassette **21** (dark red) and its analog bearing methylated BODIPY donors (blue) in a common solvent. The corresponding absorption spectra (filled) of the isolated building blocks are also added for comparison. Theoretically simulated energy arrangement of the frontier orbitals as a function of the donor alkylation in the EET cassettes is also included to illustrate the PET triggering and its ensuing emission quenching.

On the other hand, the fluorescence spectra comprise a single band (Figure 17) located at the red-edge (680-720 nm in **20** and **21**, respectively), regardless of the excitation wavelength and linkage position, owing to an efficient EET process from the peripheral BODIPY energy donors to the central energy acceptor aza-BODIPY. Despite the high efficiency of the EET process (close to 100% in view of the almost negligible emission from the donors despite its direct excitation), the fluorescence quantum yield of these cassettes depended strongly on the grafted position at the aza-BODIPY (Figure 16). In fact, linkage through the 3,5-biphenyl groups leads to brighter NIR emission than those linked directly to the boron bridge (30% vs. 8% for triads **21** and **20**, respectively). This decrease can be attributed to higher conformational freedom after tethering the donor BODIPYs to the boron bridge of the aza-BODIPYs. A similar trend was observed for dye **4** (Figure 4).

Moreover, alkylation of the donor unit also has a clear influence on the final fluorescence response of these antenna systems. In fact, this alkylation process enables a photoinduced electron transfer (PET) process upon excitation [116], which drastically quenches the fluorescence from the aza-BODIPY acceptor and entirely vanishes (Figure 17) [117]. Therefore, the alkylated BODIPYs were able to act as electron donors as well as energy donors, and the balance between both rivalling pathways could be finely triggered by modulating the HOMO energy of the donor BODIPY through their alkylation/dealkylation. Thus, non-alkylated energy donors are required to achieve glow-red emission in aza-BODIPY-based cassettes. It is noteworthy that the fluorescence efficiency of triad **21** is two-fold higher than that of its monomeric isolated precursor **18** bearing phenyl (ϕ = 0.30 *vs* ϕ = 0.12, respectively), suggesting that 3,5-biphenyls are recommended not only to further extend the π-system delocalisation, but also to restrict the conformational freedom and enhance the fluorescence signal.

Accordingly, both multichromophoric dyes **20** and **21**, which do not undergo PET, lase efficiently in the red spectral region (690 nm and 730 nm, respectively, Figure 16), regardless of the pumping wavelength (355 and 532 nm) owing to the ongoing EET. The low absorption of isolated aza-BODIPY at this pumping wavelength required high concentrations (up to 1.5 mM, in section 2.3). In contrast, the higher absorption capability of the cassettes reduced the required gain-media concentration (up to 75%), preventing dye solubility problems, reabsorption/reemission phenomena, and aggregation processes. As a result, these aza-BODIPY-BODIPY cassettes exhibit high laser efficiencies (up to 25%), outperforming their monomeric precursor (18%) under the same conditions. Regarding photostability, extremely high energy doses (145 and 142 $GJ \cdot mol^{-1}$ for **20** and **21**, respectively) are required to decrease the output emission by 10%. Again, the effectiveness of the EET process is responsible for these outstanding results. The photostable donor BODIPY receives laser

pumping and its damage, keeping the aza-BODIPY emitter excited through EET unharmed. All of these facts render a longer-lasting laser signal than its monomeric precursor **18** (energy dose of 22 GJ·mol^{-1} for the same emission loss).

3.2. All-BODIPY-based Pentads and Hexads

Styrylated BODIPYs are another suitable alternative to long-wavelength emitters and energy acceptors for customising multichromophoric cassettes. To this end, we chose dye **14** from Section 2.2, owing to its efficient (30%) and long-lasting (E_{dose} = 55 GJ/mol) red-edge (690 nm) emission. Taking it as a scaffold, a pentad was designed to graft up to four energy donor BODIPYs at the *ortho* position of the peripheral phenyls (**22**, Figure 18).

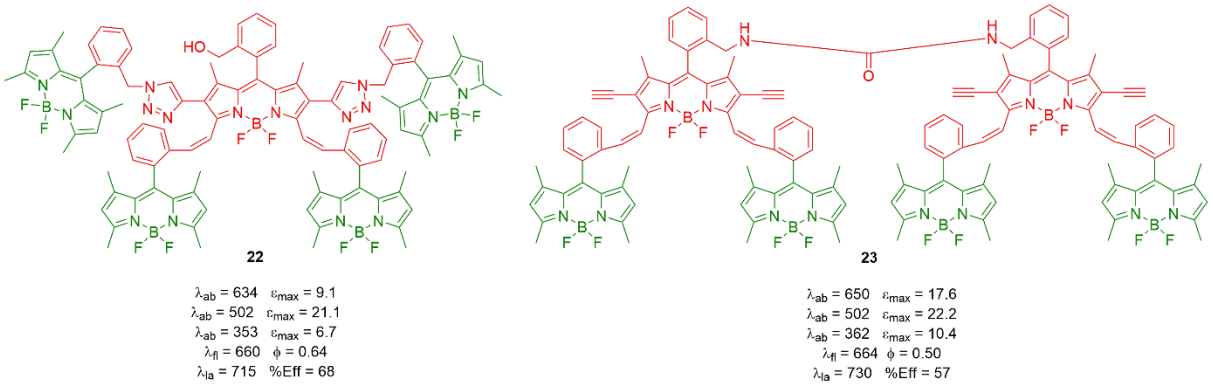

Figure 18. Molecular structure of all-BODIPY based cassettes together with their corresponding main photophysical and laser properties in ethyl acetate. Absorption (λ_{ab}) and fluorescence (λ_{fl}) wavelengths (in nm), molar absorption (ε_{max}, in $10^4 \cdot M^{-1}$ cm^{-1}), fluorescence quantum yield (ϕ), laser wavelength (λ_{la}, in nm) and efficiency (%Eff).

Furthermore, a similar triad bearing the said central red BODIPY and two tethered green BODIPYs at positions 3 and 5 dimerised through the *ortho* 8-benzyl position of the former, leading to hexad **23** (Figure 18). This pair of conformationally restricted cassettes enabled us to ascertain the role of the number of donors and acceptors (4 vs. 1 in **22** and 4 vs. 2 in **23**) in the photonic properties of the multichromophoric dyes.

The absorption spectra of cassettes **22** and **23** featured three well-defined bands (Figure 19). The band at the lowest energy (around 630-655 nm if triazole is replaced by acetylene) belongs to the π-extended central subunit. In hexad **23,** which has two π-extended central BODIPYs, this band is very strong (molar absorption coefficient of up to 170000 $M^{-1}\cdot cm^{-1}$). The most intense absorption band around 505 nm was assigned to the peripheral tetramethylated BODIPYs, whose intensity correlated with the number of BODIPY donors, reaching a molar absorption coefficient higher than 200000 $M^{-1}\cdot cm^{-1}$. Finally, the band with the lowest molar absorption probability and at the lowest wavelength is attributed to the aforementioned interaction between the styryl groups at positions 3 and 5 and the pyrrole groups of the central BODIPY (see Section 2.2) [97]. Therefore, this panchromatic absorption indicates that each chromophore retains its molecular identity after covalent linkage and contributes additively to the entire profile. In this regard, the steric hindrance around the acceptor and donor connections (involving the *ortho* position of the *meso* aryl substituent with the adjacent positions 1 and 7 methylated) is a key structural issue for fixing orthogonal orientations and avoiding excitonic couplings between chromophoric fragments.

As a result of the expected efficient intramolecular EET (> 98%), the fluorescence spectra displayed a single band at the red edge (around 660-665 nm), regardless of the excitation wavelength and the number and arrangement of the building blocks. The fluorescent efficiency ranges from 0.50 for the hexad to 0.64 for the pentad in apolar or low polarity media (Figure 18). The emission drops drastically in the most polar media, suggesting the activation of ICT processes that quench fluorescence. This finding was somehow expected in hexad **23,** since the urea spacer is able to induce ICT processes, explaining its lower fluorescent response, but was unexpected for pentad **22**, since the fluorescence efficiency of the corresponding isolated red-emitting dye **14** was not sensitive to the solvent. By analysing the counterpart triads of pentad **22**, valuable information can be

drawn about the role of the linkage position of the donors at the acceptor in the ICT probability. Thus, the triad bearing only energy donors at the 3,5-styryls showed similar solvent effect on the fluorescence efficiency than hexad **23**. However, as such donors are grafted to 2,6-triazoles, the resulting triad shows a lower dependence on the solvent polarity, retaining 45% efficiency in polar methanol. This finding points to the functionalization of the 3,5-styryl groups as the source of stabilisation of the competing ICT process between BODIPY themselves.

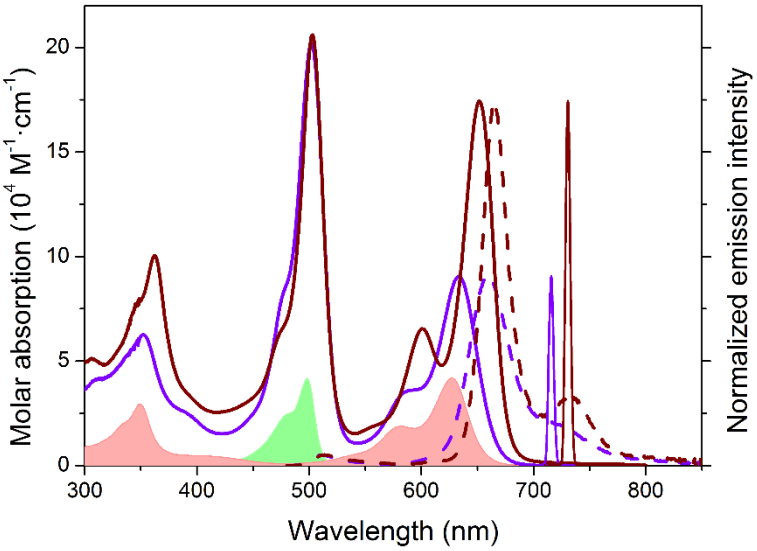

Figure 19. Absorption (solid lines), fluorescence (dashed lines, after selective excitation at the BODIPY donor) and laser spectra of cassettes **22** (violet) and **23** (dark red) in a common solvent. The corresponding absorption spectra (filled) of the isolated building blocks are also added for comparison.

In view of the broadband absorption and ongoing EET, the laser properties were studied under transverse pumping at 355 nm and 532 nm (Figure 20). Owing to the high number of energy donors with strong absorption at the pumping wavelengths, the optimal concentration of the gain medium for the highest laser efficiency was considerably lower than that of the isolated red-emitting dye **14**. The lasing emission signal is located at the NIR edge (710–730 nm, Figure 19) with remarkably high efficiency (up to 68%) and extremely

improved photostability values (up to 1140 GJ·mol^{-1}, Figure 20). It is noteworthy that in this case, the pumping conditions (8 mJ per pulse and 15 Hz as pumping energy and repetition rate, respectively) were more drastic than those usually selected for the laser characterisation of BODIPY dyes (5 mJ per pulse and 10 Hz) [118]. As a result, while the number of acceptor units has a minor impact on laser efficiency, the number of donors plays a critical role, as pentads **22** and **23** exhibit efficiency and photostability up to two- and twenty-fold higher, respectively, than isolated red-emitting dye **14** (Figure 20). These outstanding lasing properties were achieved owing to the increased absorption at the pumping wavelengths, which allowed lower energy doses to surpass the losses in the gain medium. In addition, owing to the effective EET, the indirect pumping of the final red-emitting energy acceptor further contributes to a decrease in the rate of the photodegradation processes.

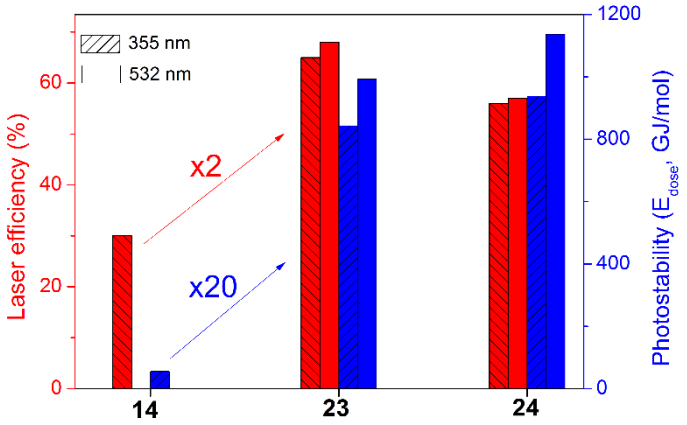

Figure 20. Lasing efficiency and photostability (defined as the amount of pumping energy absorbed by the dye to retain 50% of its initial emission) pumped at 355 nm and 532 nm of the all-BODIPY based pentad **22** and hexad **23**, and their isolated red-emitting dye **14** (only pumped at 355 nm due to its low absorption at 532 nm) under identical experimental conditions.

In brief, BODIPY- or aza-BODIPY-based energy transfer cassettes were successful in improving the photonic performance of dye lasers. They efficiently harvest the incoming pumping at different regions and display strong and exceptionally long-lasting laser emission

owing to the effectiveness of the EET process, greatly improving the performance and durability of commercial lasers in the far-red NIR window (beyond 700 nm).

Conclusions and Outlook

The rich and versatile chemistry of BODIPYs is a suitable tool for designing a library of photoactive dyes applied as efficient and stable lasers with tunable and improved emission from the green to the red edge of the visible region and approaching NIR. Laser performance can be boosted upon replacing the fluorine atoms at the boron centre of green-yellow BODIPYs with electron-withdrawing groups. To span the remaining less energetic window, π-extended BODIPYs should be designed. In particular, conformationally restricted benzofuran-fused BODIPYs are suitable for covering the orange-red region, whereas far-red-NIR-edge styryl-BODIPYs and polyarylated aza-BODIPYs are preferred. Most of the dyes described here outperform the commercially available (oxazines or cyanines) in terms of efficiency and photostability. Further enhancement of the laser properties can be achieved via covalent assembly of BODIPYs and aza-BODIPYs in a unique molecular structure. These multichromophores lead to a new generation of photoactive media with extremely long-lasting laser emissions in the red-NIR region.

Although BODIPYs have a low tendency to self-associate, an increasing number of publications have claimed that, upon appropriate chemical modifications, they can form emissive aggregates, which leads to the formation of fluorescent crystals and nanoparticles as solid-state emitters. These findings envisage a new generation of photoactive materials in the solid state, which could establish the basis for the development of BODIPY-based microlasers as alternatives to conventional lasers.

In any case, rational molecular design is critical to realising BODIPYs' full potential and endowing them with the desired photonic performance. This aim requires a deep

understanding of the structural factors governing the complex relationship between the molecular structure of the boron dipyrrin core and its photophysical properties. In this review, we aim to establish the main photophysical guidelines governing the photonic signatures of tunable dye lasers. We hope that the herein described fundamental concepts can serve as inspiration and set the basis to sketch smart and advanced organic molecules for applied photonics.

Acknowledgements

This study was supported by MINECO (PID2020-114755GB-C33) and Gobierno Vasco (IT1639-22). We would also like to acknowledge the contributions of the research groups headed by Prof. M. J. Ortiz and Prof. S. de la Moya (UCM in Madrid), Prof. J. C. López and Prof. A. Gomez (CSIC in Madrid), Prof. I. García Moreno (CSIC in Madrid), and Prof. E. Peña Cabrera (Universidad de Guanajuato in Mexico) for their fruitful collaboration in dealing with the dye chemistry of BODIPYs.

The authors report there are no competing interests to declare.

References

[1] H. Zollinger, *Color Chemistry: Syntheses, Properties and Applications of Organic Dyes and Pigments*, 3rd ed. (Wiley-VCH, Weinheim, 2003).

[2] J. R. Lakowicz, Principles of Fluorescene Spectrocospy, 2nd ed. (Springer, Boston, MA, 1999).

[3] J. F. Lovell, T. W. B. Liu, J. Chen, and G. Zheng, Chem. Rev. **110**, 2839, (2010).

[4] X. Li, S. Kolemen, J. Yoon, and E. U. Akkaya, Adv. Funct. Mater. **27**, 160405 (2017).

[5] D. Wu, A. C. Sedgwick, T. Gunnlaugsson, E. U. Akkaya, J. Yoon and T. D. James, Chem. Soc. Rev. **46,** 7105 (2017).

[6] O. Kulyk, L. Rocard, L. Maggini, and D. Bonifazi, Chem. Soc. Rev. **49,** 8400 (2020).

[7] F. de Moliner, N. Kielland, R. Lavilla, and M. Vendrell, Angew. Chem. Int. Ed. **56**, 3758 (2017).

[8] S. N. Batchelor, Color. Technol. **131**, 81 (2015).

[9] D. Bials, E. Kirchner, M. I. S. Rhör, and F. Würthner, J. Am. Chem. Soc. **143**, 4500 (2021).

[10] R. W. Sinkeldam, N. J. Greco, and Y. Tor, Chem. Rev. **110**, 2579 (2010).

[11] K. Colas, S. Doloczki, M. Posada-Urrutia, and C. Dyrager, Eur. J. Org. Chem. **15**, 2133 (2021).

[12] L. Zong, H. Zhang, Y. Li, Y. Gong, D. Li, J. Wang, Z. Wang, Y. Xie, M. Han, Q. Peng, X. Li, J. Dong, J. Qian, Q. Li, and Z. Li, ACS Nano, **12**, 9532 (2018).

[13] C. R. Lee, S. H. Lin, S. M. Wang, J. D. Lin, Y. S. Chen, M. C. Hsu, J. K. Liu, T. S. Mod and C. Y. Huang, J. Mater. Chem. C. **6**, 4959 (2018).

[14] O. Kulyk, L. Rocard, L. Maggini, and D. Bonifazi, Chem. Soc. Rev. **49**, 8400 (2020).

[15] J. H. Boyer, A. M Haag, G. Sathyamoorthi, M. L. Soong, and K. Thangaraj, Heteroat. Chem. **4**, 39 (1993).

[16] G. Sathyamoorthi, J. H. Boyer, T. H. Allik, and S. Chandra, Heteroat. Chem. **5**, 403 (1994).

[17] Z. Lin, A. W. Kohn, and T. Van Voorhis, J. Phys. Chem. C. **124**, 3925 (2020).

[18] R. Ziessel, G. Ulrich, and A. Harriman, New J. Chem. **31**, 496 (2017).

[19] J. Bañuelos, Chem. Rec. **16**, 335 (2016).

[20] M. Ahmad, T. A. King, D. K. Ko, B. H. Cha, and J. Lee, Opt. Comm. **203**, 327 (2002).

[21] B. Hinkeldey, A. Schimitt, and G. Jung, ChemPhysChem. **9**, 2019 (2008).

[22] A. P. Demchenko, Methods Appl. Fluoresc. **8**, 022001 (2020).

[23] A. A. Goorman, I. Hamblett, T. A. King, and M. D. Rahn, J. Photochem. Photobiol. A. **130**, 127 (2000).

[24] M. A. H. Alamiry, A. Harriman, A. Haefele, and R. Ziessel, ChemPhysChem, **16**, 1867 (2015).

[25] F. López-Arbeloa, T. López-Arbeloa, and I. López-Arbeloa, J. Photochem. Photobiol. A. **121**, 177 (1999).

[26] H. Manzano, I. Esnal, T. Marqués-Matesan, J. Bañuelos, I. López-Arbeloa, M. J. Ortiz, L. Cerdán, A. Costela, I. García-Moreno, and J. L. Chiara, Adv. Funct. Mater. **26**, 2756 (2016).

[27] M. Wang, M. G. H. Vicent, D. Mason, and P. Bobadova-Parvanova, ACS Omega, **3**, 5502 (2018).

[28] A. M. Gómez, J. C. López, Chem. Rec. **21**, 3112 (2021).

[29] N. Boens, B. Verbelen, M. J. Ortiz, L. Jiao, and W. Dehaen, Coord. Chem. Rev. **399**, 213024 (2019).

[30] P. Lu, K. Y. Chung, A. Stafford, M Kiker, K. Kafle, and Z. A. Page, Polym. Chem. **12**, 327 (2021).

[31] W. Sheng, F. Lv, B. Tang, E. Hao, and L. Jiao, Chin. Chem. Lett. **30**, 1825 (2019).

[32] R. G. Clarke, and M. J. Hall, *Advances in Heterocyclic Chemistry, Recent Development in the synthesis of BODIPY Dyes*, (Elsevier, Cambridge, 1st ed. 2019**)**.

[33] L. Jean-Gérard, W. Vasseur, F. Scherniniski, and B. Andrioletti, Chem. Commun. **54**, 12914 (2018).

[34] N. Boens, B. Verbelen, and W. Dehaen, Eur. J. Org. Chem. **30**, 6577 (2015).

[35] L. I. Shamova, Y. V. Zatsikha, and V. N. Nemykin, Dalton Trans, **50**, 1569 (2021).

[36] A. J. C. Kuehne, and M. C. Gather, Chem. Rev. **116**, 12823 (2016).

[37] M. Poddar, and R. Misra, Coord. Chem. Rev. **421**, 213462 (2020).

[38] H. Lu, J. Mack, T. Nyokong, N. Kobayashi, and Z. Shen, Coord. Chem. Rev. **318**, 1-15 (2016).

[39] E. M. Sánchez-Carnero, A. R. Agarrabeitia, F. Moreno, B. L. Maroto, G. Muller, M. J. Ortiz, and S. de la Moya, Chem. Eur. J. **21**, 13488 (2015).

[40] P. De Bonfils, L. Péault, P. Nun, and V. Coeffard, Eur. J. Org. Chem. **12**, 1809 (2021).

[41] K. Ivaniuk, A. Pidluzhna, P. Stakhira, G. V. Baryshnikov, Y. P. Kovtun, Z. Hotra, B. F. Minaev, and H. Agren, Dyes Pigm. **175**, 108123 (2020).

[42] H. Klfout, A. Stewart, M. Elkhalifa, and H. He, ACS Appl. Mater. Interfaces, **9**, 39873 (2017).

[43] D. Wu, A. C. Sedgwick, T. Gunnlaugsson, E. U. Akkaya, J. Yoon, and T. D. James, Chem. Soc. Rev. **46**, 7105 (2017).

[44] T. Kowada, H. Maeda, and K. Kikuchi, Chem. Soc. Rev. **44**, 4953 (2015).

[45] V. N. Nguyem, J. Ha, M. Cho, H. Li, K. M. K. Swamy, and J. Yoon, Coord. Chem. Rev. **459**, 213936 (2019).

[46] Z. Shi, X. Han, W. Hu, H. Bai, B. Peng, L. Ji, Q. Fan, L. Li, and W. Huang, Chem. Soc. Rev. **49**, 7533 (2020).

[47] P. Kaur, and K. Singh, J. Mater. Chem. C. **7**, 11361 (2019).

[48] A. Turksoy, D. Yildiz, and E. U. Akkaya, Coord. Chem. Rev. **379**, 47 (2019).

[49] V. N. Nguyen, Y. Yim, S. Kim, B. Ryu, K. M. K. Swamy, G. Kim, N. Kwon, C. Y. Kim, S. Park, and J. Yoon, Angew. Chem. Int. Ed. **59**, 8957 (2020).

[50] M. L. Agazzi, M. B. Ballatore, A. M. Durantini, E. N. Durantini, and A. C. Tomé, J. Photochem. Photobiol, C. **40**, 21 (2019).

[51] C. S. Kue, S. Y. Ng, S. H. Voon, A. Kamkaew, L. Y. Chung, L. V. Kiew, and H. B. Lee, Photochem. Photobio. Sci. **17**, 1691 (2018).

[52] M. Shah, K. Thangaraj, M. L. Soong, L. T. Wolford, and J. H. Boyer, Heteroat. Chem. **1**, 389 (1990).

[53] S. C. Guggenheimer, J. H. Boyer, K. Thangaraj, M. Shah, M. L. Soong, and T. G. Pavlopoulos, Appl. Opt. **32**, 3942 (1993).

[54] A. Costela, I. García-Moreno, and R. Sastre, Phys. Chem. Chem. Phys. **5**, 4745 (2003).

[55] J. Bañuelos, V. Martín, C. F. A. Gómez-Durán, I. J. Arroyo-Córdoba, E. Peña-Cabrera, I. García-Moreno, A. Costela, M. E. Pérez-Ojeda, T. Arbeloa, and I. López-Arbeloa, Chem. Eur. J. **17**, 7261 (2011).

[56] I. Esnal, I. Valois-Escamilla, C. F. A. Gómez-Durán, A. Urías-Benavides, M. L. Betancourt-Mendiola, I. López-Arbeloa, J. Bañuelos, I. García-Moreno, A. Costela, and E. Peña-Cabrera, ChemPhysChem, **14**, 4134 (2013).

[57] N. H. Kim, and D. Kim, *Blue-emitting BODIPY dyes*, 1st ed. (IntechOpen, London, 2018**)**.

[58] H. Lu, J. Mack, Y. Yang, and Z. Shen, Chem. Soc. Rev. **43**, 4778 (2014).

[59] M. J. Ortiz, I. García-Moreno, A. R. Agarrabeitia, G. Durán-Sampedro, A. Costela, R. Sastre, F. López-Arbeloa, J. Bañuelos, and I. López-Arbeloa, Phys. Chem. Chem. Phys. **12**, 7804 (2010).

[60] A. J. C. Kuehne, and M. C. Gather, Chem. Rev. **116**, 12823 (2016).

[61] M. Benstead, G. H. Mehl, and R. W. Boyle, Tetrahedron, **67**, 3573 (2011).

[62] X. D. Jiang, J. Zhang, T. Furuyama, and W. Zhao, W.; Org. Lett. **14**, 248 (2012).

[63] A. L. Nguyen, P. Bobodova-Parvanova, M. Hopfinger, F. R. Fronczek, K. M. Smith, and M. G. H. Vicente, Inorg. Chem. **54**, 3228 (2015).

[64] G. Ulrich, C. Goze, S. Goeb, P. Retailleau, and R. Ziesse, New J. Chem. **30**, 982 (2006).

[65] E. Bodio, and C. Goze, Dyes Pigm. **160**, 700 (2019).

[66] A. M. Courtis, S. A. Santos, S. Y. Guan, A. Hnedricks, B. Ghosh, D. M. Szantai-Kis, S. A. Reis, J. V. Shah, and R. Mazitschek, Bioconjugate Chem. **25**, 1043 (2014).

[67] O. Florès, J. Pliquett, L. A. Galan, R. Lescure, F. Denat, O. Maury, A. Pallier, P. S. Bellaye, B. Collin, S. Même, C. S. Bonnet, E. Bodio, and C. Goze, Inorg. Chem. **59**, 1306 (2020).

[68] M. Wang, G. Zhang, N. E. M. Kaufman, P. Bobadova-Parvanova, F. R. Fronczek, K. M. Smith, and M. G. H. Vicente, Eur. J. Org. Chem. **8,** 971 (2020).

[69] G. Durán-Sampedro, A. R. Agarrabeitia, L. Cerdán, M. E. Pérez-Ojeda, A. Costela, I. García-Moreno, I. Esnal, J. Bañuelos, I. López-Arbeloa, and M. J. Ortiz, Adv. Funct. Mater. **23**, 4195 (2013).

[70] G. Fan, L. Yang, and Z. Chen, Front. Chem. Sci. Eng. **8**, 405 (2014).

[71] L. Yang, G. Fan, X. Ren, L. Zhao, J. Wang, and Z. Chen, Phys. Chem. Chem. Phys. **17**, 9167 (2015).

[72] K. K. Jagtap, N. Shivran, S. Mula, D. B. Naik, S. K. Sarkar, T. Mukherjee, C. K. Maity, and A. K. Ray, Chem. Eur. J. **19**, 702 (2013).

[73] B. Brizet, C. Bernhard, Y. Volkova, Y. Rousselin, P. D. Harvey, C. Goze, and F. Denat, Org. Biomol. Chem. **11**, 7729 (2013).

[74] H. Manzano, I. Esnal, T. Marqués-Matesan, J. Bañuelos, I. López-Arbeloa, M. J. Ortiz, L. Cerdán, A. Costela, I. García-Moreno, and J. L. Chiara, Adv. Funct. Mater. **26**, 2756 (2016).

[75] R. Ziessel, G. Ulrich, A. Haefele, and A. Harriman, J. Am. Chem. Soc. **135**, 11330 (2013).

[76] H. A. Abdulhadi El-Ali, J. Jing, and X. Zhang, RSC Adv. **9**, 16246 (2019).

[77] C. Ray, L. Díaz-Casado, E. Avellanal-Zaballa, J. Bañuelos, L. Cerdán, I. García-Moreno, F. Moreno, B. L. Maroto, I. López-Arbeloa, and S. de la Moya, Chem. Eur. J. **23**, 9383 (2017).

[78] G. Durán-Sampedro, I. Esnal, A. R. Agarrabeitia, J. Bañuelos, L. Cerdán, I. García-Moreno, A. Costela, I. López-Arbeloa, and M. J. Ortiz, Chem. Eur. J. **20**, 2646 (2014).

[79] C. Hansch, A. Leo, and R. W. Taft, Chem. Rev. **91**, 168 (1991).

[80] G. Bourhill, J. L. Brédas, L. T. Cheng, S. R. Marder, F. Meyers, J. W. Perry, and B. G. Tiemann, J. Am. Chem. Soc. **116**, 2619 (1994).

[81] V. Pansare, S. Hejazi, W. Faenza, and R. K. Prud'homme, Chem. Mater. **24**, 812 (2012).

[82] M. Poddar, and R. Misra, Coord. Chem. Rev. **421**, 213462 (2020).

[83] L. Yuan, W. Lin, K. Zheng, L. He, and W. Huang, Chem. Soc. Rec. **42**, 622 (2013).

[84] S. Luo, E. Zhang, Y. Su, T. Cheng, and C. Shi, Biomaterials, **32**, 7127 (2011).

[85] C. G. Geddes, *Reviews in Fluorescence, Organized assemblies probed by fluorescence spectroscopy*, 1st ed. (Springer, Berlin, **2017)**.

[86] X, Wang, and O. S. Wolfbeis, Anal. Chem. **88**, 203 (2016).

[87] I. Martenic, S. V. Eliseeva, and S. J. Petoud, J. Lumin. **189**, 19 (2017).

[88] H. A. Shindy, Dyes Pigm. **145**, 505 (2017).

[89] S. Niu, G. Ulrich, P. Retailleau, and R. Ziessel, Tetrahedron Lett. **52**, 4848 (2011).

[90] X. Wu, Y. Zhang, K. Takle, O. Bilsel, Z. Li, H. Lee, Z. Zhang, D. Li, W. Fan, C. Duan, E. M. Chan, C. Lois, Y. Xiang and G. Han, ACS Nano, **10**, 1060 (2016).

[91] E. Heyer, P. Retailleau, and Ziessel, Org. Lett. **16**, 2330 (2014).

[92] Y. Ni, and J. Wu, Org. Biomol. Chem. **12**, 3774 (2014).

[93] M. J. Hall, S. O. McDonell, J. Killoran, and D. F. O'Shea, J. Org. Chem. **70**, 5571 (2005).

[94] Y. Ge, and D. F. O'Shea, Chem. Soc. Rev. **45**, 3846 (2016).

[95] W. Freyer, S. Mueller, and K. Teuchner, J. Photochem. Photobio. **163**, 231 (2004).

[96] J. L. Belmonte-Vázquez, E. Avellanal-Zaballa, E. Enríquez-Palacios, L. Cerdán, I. Esnal, J. Bañuelos, C. Villegas-Gómez, I. López Arbeloa, and E. Peña-Cabrera, J. Org. Chem. **84**, 2523 (2019).

[97] C. F. A. Gómez-Durán, I. Esnal, I. Valois-Escamilla, A. Urías- Benavides, J. Bañuelos, I. López-Arbeloa, I. García-Moreno, and E. Peña-Cabrera, Chem. Eur. J. **22**, 1048 (2016).

[98] V. Masilamani, and A. S. Aldwayyan, Acta, Part A. **60**, 2099 (2004).

[99] L. Cerdán, V. Martínez-Martínez, I. García-Moreno, A. Costela, M. E. Pérez-Ojeda, I. López-Arbeloa, I.; L. Wu, and K. Burgess, Adv. Opt. Mater. **1**, 984 (2013).

[100] G. Durán-Sampedro, A. R. Agarrabeitia, T. Arbeloa-López, J. Bañuelos, I. López-Arbeloa, J. L. Chiara, I. García-Moreno, and M. J. Ortiz, Laser Phys. Lett. **11**, 115818 (2014).

[101] I. García-Moreno, A. Costela, V. Martín, M. Pintado-Sierra, R. Sastre, Adv. Funct. Mater. **19**, 2547 (2009).

[102] G. Jones, S. Kumar, O. Klueva, and D. Pacheco, J. Phys. Chem. A. **107**, 8429 (2003).

[103] I. García-Moreno, L. Wang, A. Costela, J. Bañuelos, I. López-Arbeloa, and Y. Xiao, ChemPhysChem. **13**, 3923 (2012).

[104] A. Prieto-Castañeda, E. Avellanal-Zaballa, L. Gartzia-Rivero, L. Cerdán, A. R. Agarrabeitia, I. García-Moreno, J. Bañuelos, and M. J. Ortiz, ChemPhotoChem, **3**, 75 (2019).

[105] P. Hewavitharanage, R. Warshawsky, S. V. Rosokha, J. Vaal, K. Stickler, D. Bachynsky, and N. Jairath, Tetrahedron, **76**, 131515 (2020).

[106] C. Azarias, R. Russo, L. Cupellini, B. Mennucci, and D. Jacquemin, Phys. Chem. Phys. Chem. **19**, 6443 (2017).

[107] N. Balsukuri, N. Manav, M. Y. Lone, S. Mori, A. Das, P. Sen, and I. Gupta, Dyes Pigm. **176**, 108249 (2020).

[108] P. K. Dutta, R. Varghese, J. Nangreave, S. Lin, H. Yan, and Y. Liu, J. Am. Chem. Soc. **133**, 11985 (2011).

[109] O. A. Goryacheva, N. V. Beloglazova, A. M. Vostrikova, M. V. Pozharov, A. M. Sobolev, and I. Y. Goryacheva, Talanta, **164**, 377 (2017).

[110] V. Saravanan, S. Ganesan, and P. Rajakumar, RSC Adv. **10**, 18390 (2020).

[111] J. L. K. Davis, R. W. MacQueen, S. T. E. Jones, C. Orofino-Pena, D. Cortizo-Lacalle, R. G. D. Taylor, D. Credgington, P. J. Skabara, and N. C. Greenham, J. Mater. Chem. C, **5**, 1952 (2017).

[112] V. Vohra, G. Calzaferri, S. Destri, M. Pasini, W. Porzio and C. Botta, ACS Nano, **4**, 1409 (2010).

[113] D. M. Coles, A. A. P. Trichet, P. R. Dolan, R. A. Taylor, C. Vallance, J. M. Smith, Laser Photonics Rev. **8**, 538 (2015).

[114] R. Mallah, M. C. Sreenath, S. Chitrambalam, I. H. Joe, N. Sekar, Optical Materials, **84**, 795 (2018).

[115] L. Cerdán, E. Enciso, V. Martín, J. Bañuelos, I. López-Arbeloa, A. Costela, and I. García-Moreno, Nat. Photonics, **6**, 621 (2012).

[116] M. E. El-Khouly, A. N. Amin, M. E. Zandler, S. Fukuzumi, and F. D'Souza, Chem. Eur. J. **18**, 5239 (2012).

[117] E. Avellanal-Zaballa, A. Prieto-Castañeda, F. García-Garrido, A. R. Agarrabeitia, E. Rebollar, J. Bañuelos, I. García-Moreno, and M. J. Ortiz, Chem. Eur. J., **26**, 16080 (2020).

[118] L. Cerdán, A. Costela, I. García-Moreno, J. Bañuelos, and I. López-Arbeloa, Laser Phys. Lett. **9**, 426 (2012).